

On the quasi-analytic treatment of hysteretic nonlinear response in elastic wave propagation

Koen E-A Van Den Abeele,^{a)} Paul A. Johnson,^{b)} Robert A. Guyer,^{c)}
and Katherine R. McCall^{d)}

EES-4, MS D443, and IGPP, Los Alamos National Laboratory, Los Alamos, New Mexico 87545

(Received 10 May 1996; revised 11 November 1996; accepted 14 November 1996)

Microscopic features and their hysteretic behavior can be used to predict the macroscopic response of materials in dynamic experiments. Preisach modeling of hysteresis provides a refined procedure to obtain the stress–strain relation under arbitrary conditions, depending on the pressure history of the material. For hysteretic materials, the modulus is discontinuous at each stress–strain reversal which leads to difficulties in obtaining an analytic solution to the wave equation. Numerical implementation of the integral Preisach formulation is complicated as well. Under certain conditions an analytic expression of the modulus can be deduced from the Preisach model and an elementary description of elastic wave propagation in the presence of hysteresis can be obtained. This approach results in a second-order partial differential equation with discontinuous coefficients. Classical nonlinear representations used in acoustics can be found as limiting cases. The differential equation is solved in the frequency domain by application of Green’s function theory and perturbation methods. Limitations of this quasi-analytic approach are discussed in detail. Model examples are provided illustrating the influence of hysteresis on wave propagation and are compared to simulations derived from classical nonlinear theory. Special attention is given to the role of hysteresis in nonlinear attenuation. In addition guidance is provided for inverting a set of experimental data that fall within the validity region of this theory. This work will lead to a new type of NDT characterization of materials using their nonlinear response. © 1997 Acoustical Society of America. [S0001-4966(97)01304-0]

PACS numbers: 43.25.Dc [MAB]

INTRODUCTION

Nature accommodates some bizarre and unique elastic systems. Static stress–strain tests on rocks, for instance, illustrate their extremely nonlinear response, including both hysteresis and end point memory.^{1–8} The principal theoretical component in static and dynamic studies is the equation of state (EOS), which relates stress to strain. In the case of rocks (and some other materials, such as shape memory alloys,⁹ PZTs,^{10,11} etc.), the deformation is a complex multi valued function of the external stress (hysteresis) and of the history of its changes (memory): in fact, rocks can be considered as systems having an infinite number of state relations. It is the EOS that we must understand in order to describe the dynamic response of rock.

Initially, nonlinear elasticity models were based on theory derived from the domain of nonlinear fluid acoustics.^{12,13} A first-order perturbation expansion of the modulus or velocity in terms of the strain is incorporated into the wave equation to describe nonlinear effects such as wave distortion and the corresponding generation of harmonics.

With the modulus depending on the excited strain levels, the stress–strain relation becomes nonlinear, too. It is important to note that this model has worked very well for ordinary materials that exhibit small nonlinear response.¹⁴ It is not appropriate for most rocks, however. In a number of papers by our group at Los Alamos, we generalized the stress–strain relation to include higher-order anharmonicity and applied the results to rock dynamics. Both wave propagation and resonance experiments under different conditions have been evaluated using the generalized expansion theory.^{8,15–20} From the standpoint of an overview of numerous experiments on rock over a broad frequency and strain interval,²¹ we conclude that classical perturbation theory is incorrect or at least incomplete. Coefficients of nonlinearity deduced from dynamic studies do not agree with static predictions, and display amplitude dependence in simulations of a set of experimental wave propagation data.¹⁸ In resonance experiments on rock, classical perturbation theory of a “Duffing-type” resonating particle predicts an incorrect dependence of the frequency shift on the measured acceleration.^{8,20} The reason for these discrepancies is that the traditional theory makes no attempt to describe experiments that show hysteresis. With rocks, a rather complex picture emerges. Experimental evidence suggests that hysteresis and end point memory are omnipresent even at dynamic levels, calling for a discontinuous model of the equation of state as an alternative and more physically realistic approach. It is the microscopic structure (cracks, grain-to-grain boundaries, etc.) of

^{a)}Also Post-Doctoral Research Fellow of the Belgian Foundation for Scientific Research, Catholic University Leuven Campus Kortrijk (Interdisciplinary Research Center), Kortrijk, Belgium, and presently at Los Alamos National Laboratory on a NATO Advanced Fellowship.

^{b)}Also at Université Pierre et Marie Curie, Laboratoire d’Acoustique Physique, Paris, France.

^{c)}Also at Department of Physics and Astronomy, University of Massachusetts, Amherst, MA.

^{d)}Also at Department of Physics, University of Nevada, Reno, NV.

the elastic features and their hysteretic behavior that determines the macroscale nonlinear response.

McCall and Guyer have introduced a new model of rock elasticity and developed this model in a series of papers.^{7,8,22,23} As McCall and Guyer noted, the basic idea behind the model is presented in earlier work of Walsh²⁴ and Holcomb.¹ This approach takes the elastic properties of a macroscopic sample of material to result from the workings of a large number of mesoscopic elastic elements (on the order of 10^{12} in a cubic centimeter). These elastic elements can individually have complex hysteretic behavior. The most important portion of the theory is the Preisach–Mayergoyz (P–M) space, which provides an infinite number of state relations by tracking the behavior of the individual elastic elements depending on the excitation and the pressure history. The theory reduces to the traditional theory in the limit of no hysteresis and no discrete memory, and—as a consequence of its greater generality—is more difficult to apply. We refer the reader to Refs. 7 and 22 for a full description of the P–M model for rocks.

In this paper we focus on a (quasi-)analytic approach of the P–M space in connection to the wave propagation equation. Our goal is to achieve a *dynamic* calculation for application to wave propagation in rocks using input data from a P–M space density found empirically from *static* tension-compression measurements. The major difficulty in obtaining an analytic solution is in addressing discontinuities in the modulus–strain relation (see details later). Simple approximations will be made concerning the P–M space in order to treat the problem quasi-analytically. Doing so, the modified nonlinear wave equation, which includes hysteresis and discrete memory in the equation of state, translates into a differential equation with discontinuous coefficients. To a certain extent the solution can be obtained by avoiding the discontinuity and interpreting the problem in the Fourier domain. This problem has been briefly illustrated by McCall and Guyer²³ and will be elaborated on in this paper. Examples will be provided showing the effects of hysteresis and discrete memory on the dynamic wave propagation behavior in combination with traditional nonlinearity. We carefully study the influence of hysteresis on the waveform and its harmonic spectra, on attenuation properties, and on the functional distance, source amplitude, and frequency dependencies of harmonics. We conclude by discussing the limits of the analytic treatment and address the complexity of numerical modeling involving the integral P–M space.

I. THEORY AND LIMITATIONS

In this section we start with the classical nonlinear wave equation from acoustics. This is followed by incorporating an analytic formulation of hysteresis resulting from P–M space considerations. We will show that, to first order, hysteresis introduces a discontinuous term in the wave equation. The solution for this equation can be obtained by application of Green’s function and perturbation methods. We explicitly derive the solution for a continuous source signal with an arbitrary (discrete) frequency spectrum. Finally, we indicate the limitations of this quasi-analytic approach in connection to the Fourier transformation of the discontinuous term.

Because our laboratory bench top experiments involving wave propagation are usually performed in small diameter cylindrical bars by exciting the lowest-order Pochhammer mode (or Young’s mode),¹⁵ we can simplify the problem to a one-dimensional description using a wave equation of the following type:

$$\rho_0 \frac{\partial^2 u}{\partial t^2} = M_2(1 + \kappa(x, t)) \frac{\partial^2 u}{\partial x^2} + S(x, t). \quad (1)$$

Here S is the source function, u is the particle displacement at Lagrangian position x and time t , ρ_0 is the unstrained density of the medium, M_2 is the linear Young’s modulus (a combination of second order elastic constants equal to $\rho_0 c_0^2$ where c_0 is the linear velocity), and $\kappa(x, t)$ is the ratio of the nonlinear to linear contributions to the modulus.

Traditional theoretical models simply make use of a series expansion expression of $\kappa(x, t)$ in terms of the strain $\varepsilon = \partial u / \partial x$, introducing nonlinear coefficients in the equation of state. In this case,

$$\kappa(x, t) = \beta \frac{\partial u}{\partial x} + \delta \left(\frac{\partial u}{\partial x} \right)^2 + \dots, \quad (2)$$

where $\beta = M_3 / M_2$ and $\delta = M_4 / M_2$. Here, M_3 and M_4 are, respectively, linear combinations of second- and third-order elastic constants, and second-, third-, and fourth-order constants, in the direction of propagation.

Classical nonlinear theory generally does a poor job in predicting behavior in rock. As shown and discussed in one of our previous papers,¹⁸ the application of the traditional nonlinear model including cubic anharmonicity to experimental data results in nonlinearity parameters with magnitudes that are difficult to justify when compared to static stress–strain test predictions. In particular, the cubic anharmonicity term, which arises from nonzero fourth-order elastic constants, is two to three orders of magnitude larger than its estimation based on static measurements. Also, we noticed a systematic amplitude dependence of the nonlinearity coefficients indicating that the assumptions of the model are incorrect and that the theory is at the very least incomplete. Finally, classical nonlinear models do not display the multi-valued state relations as predicted by comprehensive static stress–strain test, i.e., excursions up and down in pressure.

Convinced by the large number of experimental observations illustrating the presence of hysteresis and discrete memory in rocks over a broad interval in frequency and strain,^{1–6} McCall and Guyer developed a new theoretical paradigm for the description of the elastic behavior of rocks.^{7,22,23} This alternative model is based on the Preisach model for hysteresis²⁵ and uses Mayergoyz’ ideas²⁶ to translate the properties of the microscopic structure, i.e., the nature of the compliant portion of the material (grain to grain contacts, cracks, contained fluids, etc.), into the macroscopic behavior of the rock using effective medium theory. In the model, the fundamental building blocks are the individual hysteretic mesoscopic elastic units [HMEU, Fig. 1(a)] assembled into the Preisach–Mayergoyz (or P–M) space which represents the density of individual HMEU’s [Fig. 1(b)]. The P–M space is a pressure–pressure space (P_c, P_0). As illustrated in Fig. 1(a), the closing pressure P_c corre-

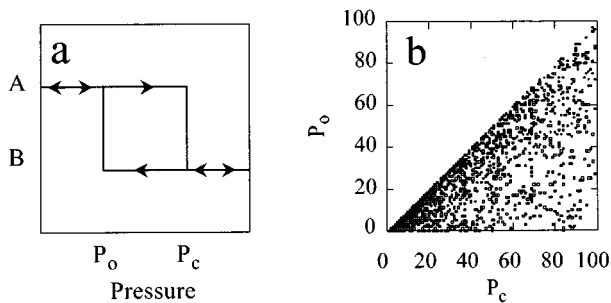


FIG. 1. (a) Representation of a hysteretic mesoscopic elastic unit (HMEU). (b) Typical P–M space representing the density of HMEU’s in a sample.

sponds to the pressure at which a HMEU changes from state A to state B while increasing the pressure. The opening pressure P_0 then represents the pressure at which the same feature changes from state B back to its initial state A while decreasing the pressure. A large number of the HMEU’s with differing P_c, P_0 comprise a model of the compliant features of a sample material. The P–M space is constructed by plotting the characteristic (P_c, P_0) pressures for the individual HMEU’s and filling the lower triangular half-space ($P_c \geq P_0$) as seen in Fig. 1(b). Nonhysteretic units (i.e., $P_c = P_0$) are on the diagonal, and hysteretic units fall in the bottom triangle in P–M space. The more hysteretic a HMEU is, the farther from the diagonal it resides. Using statistics, a density of compliant features can be associated to each point of the P–M space, given by $\rho(P_c, P_0)$. It is beyond the scope of this paper to review this model in more detail. We refer the reader to the extensive work of our colleagues.^{7,22,23}

The P–M space representation with its associated density can be used to construct realistic stress–strain curves that include hysteresis and discrete memory and that model static observations very well. Static pressure excursions sample different volumes of HMEU’s for increasing or decreasing pressure. This results in typical hysteresis loops showing discontinuities and discrete memory in the equation of state depending on the pressure path. Based on laboratory observations it is reasonable to assume that dynamic excursions also display hysteresis and discrete memory. In the following we will describe how $\kappa(x, t)$, the ratio of nonlinear to linear moduli in Eq. (1), can be obtained for dynamic experiments using very simple assumptions about the P–M space density in the region of interest. This will provide us the tools to correctly model dynamic observations.

Suppose we simulate a wave propagation experiment in which the source is a sequence of sinusoidal oscillations, or identically pressure excursions of amplitude ΔP , centered at average pressure \bar{P} . Because ΔP in dynamic excursions is very small, two assumptions can be made: (1) The P–M density of the nonhysteretic elastic features on the diagonal of Fig. 1(b) (which corresponds to the major percentage of the P–M density) can be expanded in the pressure deviation p around \bar{P} , where $p = P - \bar{P}$, and $-\Delta P \leq p \leq \Delta P$. (The pre-supposition of a series expansion will enable us to easily obtain analytic solutions and to retrieve the classical nonlinear theory formalism as a special case.) (2) The P–M density

of the hysteretic elastic units off the diagonal ($P_c < P_0$) is considered constant (uniform background) near the diagonal. This yields the following approximate expression for the P–M density $\rho(P_c, P_0)$ in the case of a dynamic wave experiment:

$$\rho(P_c, P_0) = [a_0 + a_1 p + a_2 p^2 + \dots] \cdot \hat{\delta}(P_0 - P_c) + \hat{\rho}_B, \quad (3)$$

where $\hat{\rho}_B$ is the constant P–M space density off the diagonal in the pressure region of interest, and $\hat{\delta}(\bullet)$ is the delta distribution function. The P–M space density given in Eq. (3) is expressed in units of P^{-2} . Therefore, $\hat{\rho}_B$ also has units of P^{-2} , and because a delta function has units inversely proportional to its argument, a_0 must be expressed in units of P^{-1} , a_1 in units of P^{-2} , and a_2 in units of P^{-3} .

Following equations 28–32 in McCall and Guyer’s derivation of the modulus from the P–M space density,²² the inverse elastic modulus then corresponds to

$$\frac{1}{M} = \xi_0 [a_0 + a_1 p + a_2 p^2 + \dots + \hat{\rho}_B (\Delta P \pm p)], \quad (4)$$

where the plus sign corresponds to the (inverse) modulus for increasing pressure and the minus sign for decreasing pressure. Here ξ_0 is a dimensionless constant that can be found from experiment. Assuming p and ΔP are small, Eq. (4) can be inverted to find the following first-order expression for the modulus. Identifying the constant pressure independent contribution with the “linear” dynamic modulus M_2 gives

$$M = [M_2 + b_1 p + b_2 p^2 - \rho_B (\Delta P \pm p) + \dots] \quad (5)$$

(b_1, b_2 , and ρ_B can be calculated from the inversion using a Taylor series expansion). The last step consists of the substitution of the relationship between pressure and strain to first order in Eq. (5) (Hooke’s law $p = -M_2 \varepsilon = -M_2 \frac{\partial u}{\partial x}$, and $\Delta P = M_2 \Delta \varepsilon = M_2 \Delta \frac{\partial u}{\partial x}$ with $\Delta \varepsilon$ or $\Delta \frac{\partial u}{\partial x}$ being the maximum strain excursion), which results in

$$M = M_2 \left[1 + \beta \frac{\partial u}{\partial x} + \delta \left(\frac{\partial u}{\partial x} \right)^2 - \rho_B \left(\Delta \frac{\partial u}{\partial x} \pm \frac{\partial u}{\partial x} \right) + \dots \right] \quad (6)$$

with $\beta = -b_1$ and $\delta = b_2 M_2$. Here, β, δ , and ρ_B are dimensionless parameters. The plus sign corresponds to the modulus for increasing strain and the minus sign for decreasing strain. It must be noted that this substitution is only correct under the assumption that dissipation does not contribute to the forces to first order. We will return later to the subject of attenuation.

Equation (6) gives the formulation of the dynamic modulus resulting from rudimentary P–M space considerations. In view of Eq. (1), we can identify the ratio of the nonlinear to linear contributions to the modulus, $\kappa(x, t)$, as

$$\kappa(x, t) = \beta \frac{\partial u}{\partial x} + \delta \left(\frac{\partial u}{\partial x} \right)^2 - \rho_B \left(\Delta \frac{\partial u}{\partial x} \pm \frac{\partial u}{\partial x} \right) + \dots \quad (7)$$

It is clear that the elastic modulus is hysteretic for $\rho_B \neq 0$. For $\rho_B = 0$, the modulus is a power series in the strain and does not differ for increasing or decreasing strain. In this case the model reverts to the traditional theory corresponding to Eq. (2).

As a first approximation, the P–M paradigm for rocks accounts for hysteresis and end point memory by introducing a discontinuous term in the dynamic modulus. The elastic modulus depends not only on the instantaneous value of the strain but also on its amplitude and the reversal points at each extremum. This complicates the manipulation of the wave equation significantly. The problem becomes a differential equation with discontinuous coefficients that are functions of the dependent variable by its derivatives and their amplitude. A quasi-analytic solution can be obtained using a Green’s function formalism in combination with perturbation theory.^{16,17,23} We illustrate this in the following.

We write the solution to the nonlinear wave equation as the sum of the zeroth-order “linear” displacement [$u^{(0)}(x,t)$] and a nonlinear contribution [$u^{(1)}(x,t)$], and we assume that every nonlinear term in $\kappa(x,t)$ [Eq. (7)] contributes as a first-order perturbation to the linear solution. In a previous paper we proved that higher-order terms can be accounted for by performing small iteration steps in distance, i.e., using a variant of the finite difference procedure.¹⁷ Using Green’s function theory, the Fourier transformation of the linear displacement component satisfies

$$\begin{aligned} \tilde{u}^{(0)}(x,\omega) &= \int_{-\infty}^{+\infty} dt u^{(0)}(x,t) e^{i\omega t} \\ &= \int_{-\infty}^{+\infty} dx' \frac{e^{i(\omega/c_0)cq(\omega)|x-x'|}}{-2i(\omega/c_0)cq(\omega)} \cdot \frac{\tilde{S}(x',\omega)}{M_2}, \end{aligned} \quad (8)$$

where $c_0 = \sqrt{M_2/\rho_0}$ is the linear velocity, and $\tilde{S}(x,\omega)$ is the Fourier transformation of the source function. The factor $cq(\omega)$ equals $(1+i\text{sign}(\omega)/2Q)$, and is an *ad hoc* manner in which we introduce intrinsic attenuation, linear with frequency, for a given quality factor Q .

Our primary interest in this paper lays in the investigation of nonlinear distortion of propagating pulsed waves. Therefore we can specify $\tilde{S}(x,\omega)$ by its discrete Fourier spectrum. Assuming a “breathing” mode source where the source expands symmetrically about its vertical axis [i.e., $u(-x,t) = -u(x,t)$],

$$\begin{aligned} \tilde{S}(x,\omega) &= \int_{-\infty}^{+\infty} dt S(x,t) e^{i\omega t} \\ &= -2M_2 \frac{\partial[\hat{\delta}(x)]}{\partial x} \cdot 2\pi \sum_{n=-\infty}^{+\infty} U_n \hat{\delta}(\omega - n\omega_0) \end{aligned} \quad (9)$$

in which ω_0 is the fundamental source frequency, and $U_n = [U_{-n}]^*$ is a complex number describing the amplitude A_n and phase ϕ_n of the n th harmonic displacement component at $x=0$, i.e., $U_n = -(i/2)A_n e^{i\phi_n}$, and again, $\hat{\delta}(\bullet)$ is the delta distribution function. In this case $\tilde{u}^{(0)}(x,\omega)$ becomes

$$\tilde{u}^{(0)}(x,\omega) = 2\pi \frac{x}{|x|} \sum_{n=-\infty}^{+\infty} U_n \hat{\delta}(\omega - n\omega_0) e^{i(\omega/c_0)cq(\omega)|x|}. \quad (10)$$

The first-order perturbation contribution to the solution satisfies the following linear differential equation:

$$\begin{aligned} \left[\frac{\partial^2}{\partial x^2} + \frac{\omega^2}{c_0^2} \right] \tilde{u}^{(1)}(x,\omega) &= -\beta \int_{-\infty}^{+\infty} \frac{\partial u^{(0)}}{\partial x}(x,t) \cdot \frac{\partial^2 u^{(0)}}{\partial x^2}(x,t) e^{i\omega t} dt \\ &\quad - \delta \int_{-\infty}^{+\infty} \left[\frac{\partial u^{(0)}}{\partial x}(x,t) \right]^2 \cdot \frac{\partial^2 u^{(0)}}{\partial x^2}(x,t) e^{i\omega t} dt \\ &\quad + \rho_B \int_{-\infty}^{+\infty} \left[\Delta \left(\frac{\partial u^{(0)}}{\partial x} \right) \pm \frac{\partial u^{(0)}}{\partial x}(x,t) \right] \\ &\quad \cdot \frac{\partial^2 u^{(0)}}{\partial x^2}(x,t) e^{i\omega t} dt. \end{aligned} \quad (11)$$

As seen from this equation, the source for $u^{(1)}(x,t)$ is composed of three nonlinear contributions in $u^{(0)}(x,t)$ and its derivatives which identify the nonconstant distribution of HMEU’s on the diagonal in P–M space and the nonzero background value off the diagonal. The third term on the right-hand side of Eq. (11) contains the discontinuity introduced by hysteresis considerations. The switching between plus and minus occurs at each strain reversal in time. Obtaining an analytic solution to Eq. (11) is problematic because of this discontinuity. One can sidestep this difficulty by approximating the function $[\Delta(\partial u^{(0)}/\partial x) \pm \partial u^{(0)}/\partial x](x,t)$ [which we rename $H_0(x,t)$ in the following] using its discrete Fourier series expansion. Suppose $\{h_m\}$ are the complex Fourier coefficients of this function. Then

$$\begin{aligned} H_0(x,t) &= \left[\Delta \left(\frac{\partial u^{(0)}}{\partial x} \right) \pm \frac{\partial u^{(0)}}{\partial x} \right](x,t) \\ &= \sum_{m=-\infty}^{+\infty} h_m e^{im(\omega_0/c_0)cq(\omega)|x| - im\omega_0 t} \end{aligned} \quad (12)$$

from which

$$\tilde{H}_0(x,\omega) = 2\pi \sum_{m=-\infty}^{+\infty} h_m e^{i(\omega/c_0)cq(\omega)|x|} \hat{\delta}(\omega - m\omega_0). \quad (13)$$

Rearranging integrands in Eq. (11) by use of the convolution rule for Fourier transformations and subsequent application of the Green’s function theory yields the following general solution for $\tilde{u}^{(1)}(x,\omega)$:

$$\begin{aligned}
\tilde{u}^{(1)}(x, \omega) = & \frac{\beta}{2\pi} \int_{-\infty}^{+\infty} dx' \frac{e^{i(\omega/c_0)cq(\omega)|x-x'|}}{-2i(\omega/c_0)cq(\omega)} \cdot \int_{-\infty}^{+\infty} \frac{\partial \tilde{u}^{(0)}}{\partial x'}(x', \omega') \cdot \frac{\partial^2 \tilde{u}^{(0)}}{\partial x'^2}(x', \omega - \omega') d\omega' \\
& + \frac{\delta}{(2\pi)^2} \int_{-\infty}^{+\infty} dx' \frac{e^{i(\omega/c_0)cq(\omega)|x-x'|}}{-2i(\omega/c_0)cq(\omega)} \cdot \int_{-\infty}^{+\infty} \int_{-\infty}^{+\infty} \frac{\partial \tilde{u}^{(0)}}{\partial x'}(x', \omega') \cdot \frac{\partial \tilde{u}^{(0)}}{\partial x'}(x', \omega'') \\
& \quad \cdot \frac{\partial^2 \tilde{u}^{(0)}}{\partial x'^2}(x', \omega - \omega' - \omega'') d\omega' d\omega'' \\
& - \frac{\rho_B}{2\pi} \int_{-\infty}^{+\infty} dx' \frac{e^{i(\omega/c_0)cq(\omega)|x-x'|}}{-2i(\omega/c_0)cq(\omega)} \cdot \int_{-\infty}^{+\infty} \tilde{H}_0(x', \omega') \cdot \frac{\partial^2 \tilde{u}^{(0)}}{\partial x'^2}(x', \omega - \omega') d\omega'. \tag{14}
\end{aligned}$$

Substituting the expression for $\tilde{u}^{(0)}(x, \omega)$ [Eq. (10)] and the Fourier transformation of $H_0(x, t)$ [Eq. (13)] in Eq. (14) and working through the immense job of analytically calculating the integrals we obtain a general expression describing the harmonic distortion of a pulsed signal propagated over a distance x in an elastically nonlinear and hysteretic medium. However, because this expression is obtained using perturbation theory, it is restricted in its analytic form to small distances x from the source. For large distances L , the distortion must be calculated by a finite difference or iterative procedure.^{17,27,28} Therefore we divide the total distance L into N intervals, each of length $\Delta x = L/N$. The calculated signal at the beginning of each interval is used as the source for the computation of the waveform and spectrum propagating over the next interval L/N . As illustrated in our previous papers, frequency-dependent attenuation can be accounted for at each step in the iteration. In terms of the strain components

$$\begin{aligned}
\varepsilon_n(x) = & i \frac{n\omega_0}{c_0} cq(n\omega_0) U_n(x) \\
= & n \frac{\omega_0}{2c_0} cq(n\omega_0) A_n(x) \exp[i\phi_n(x)], \tag{15}
\end{aligned}$$

the perturbation solution at $x_0 + \Delta x$, based on the virtual ‘source’ at x_0 , for each frequency component is given by

$$\begin{aligned}
\varepsilon_n(x_0 + \Delta x) = & \varepsilon_n(x_0) \exp\left[i \frac{n\omega_0}{c_0} cq(n\omega_0) |\Delta x| \right] \\
& + i \frac{\Delta x}{|\Delta x|} \frac{\omega_0}{2c_0} \sum_{m=-\infty}^{+\infty} (n-m) \cdot cq((n-m)\omega_0) \\
& \cdot \varepsilon_{n-m}(x_0) \cdot \text{Int}(n, m, n-m, 0) \cdot [-\beta \varepsilon_m(x_0) \\
& + \rho_B h_m(x_0)] - i \delta \frac{\Delta x}{|\Delta x|} \frac{\omega_0}{2c_0} \sum_{m, l=-\infty}^{+\infty} l \\
& \cdot cq(l\omega_0) \cdot \varepsilon_{n-m-l}(x_0) \cdot \varepsilon_m(x_0) \cdot \varepsilon_l(x_0) \\
& \cdot \text{Int}(n, n-m-l, m, l). \tag{16}
\end{aligned}$$

where

$$\text{Int}(n_1, n_2, n_3, n_4) = 2k_1 \frac{e^{ik_1|\Delta x|} - e^{ik_{234}|\Delta x|}}{i(k_1^2 - k_{234}^2)}$$

with

$$k_1 = \frac{n_1\omega_0}{c_0} cq(n_1\omega_0)$$

and

$$\begin{aligned}
k_{234} = & \frac{n_2\omega_0}{c_0} cq(n_2\omega_0) + \frac{n_3\omega_0}{c_0} cq(n_3\omega_0) \\
& + \frac{n_4\omega_0}{c_0} cq(n_4\omega_0). \tag{17}
\end{aligned}$$

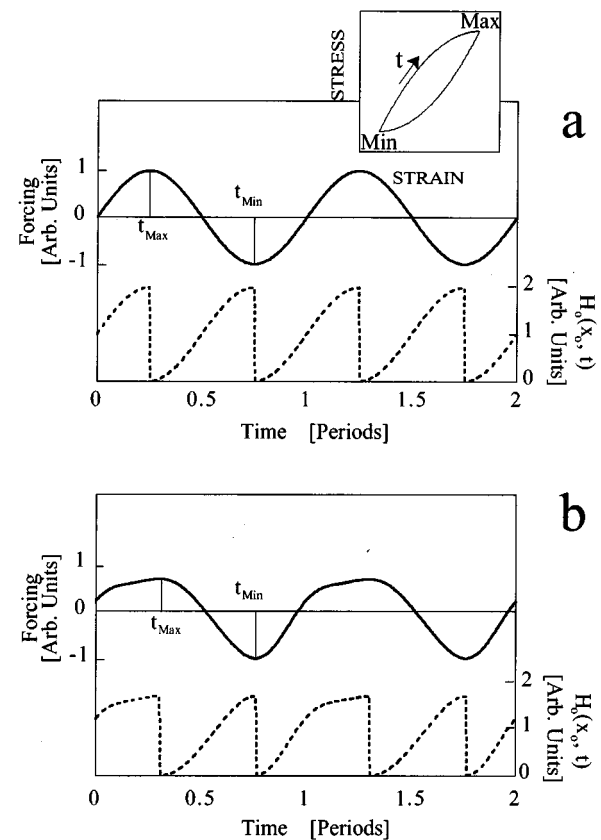


FIG. 2. Examples of the function $H_0(x, t)$ (the discontinuous portion of the nonlinear modulus) for a pure monofrequency (a) and a moderately distorted (b) sinusoidal ‘simplex’ wave forcing function representative for an equation of state with one major stress–strain hysteresis loop (see inset).

The discontinuous function $H_0(x,t)$ and its Fourier transformation $\tilde{H}_0(x,\omega)$ pose rather severe restraints as to the extent on which this problem can be solved analytically (or better quasi-analytically). In the case of a periodic monofrequency sinusoidal time history for the strain, McCall and Guyer,²³ proved that only even Fourier coefficients in Eqs. (12) and (13) are nonzero, resulting eventually in the creation of odd harmonics in the distorted spectrum along the propagation path. However, the analytic representation of the nonlinear part of the modulus given by McCall and Guyer is only valid for a pure single frequency sinusoidal forcing function. As the propagation path increases, the local strain becomes progressively distorted, its maximum and minimum change (not necessarily symmetrically) and are shifted in time (not necessarily separated by half a period). Multiple maxima and minima may be observed during one period. In these cases the analytic expressions for the Fourier coefficients of $H_0(x,t)$ generally become far more elaborate. As long as the strain has a periodic time history with only one maximum and one minimum per period, which we will de-

fine as “simplex wave” henceforth, one can proceed with the following algebraic formulas:

$$H_0(x,t) = \begin{cases} \frac{\partial u^{(0)}}{\partial x}(x,t) - \left(\frac{\partial u^{(0)}}{\partial x}\right)_{\text{Min}} & \text{if } \frac{\partial^2 u^{(0)}}{\partial t \partial x}(x,t) \geq 0, \\ \left(\frac{\partial u^{(0)}}{\partial x}\right)_{\text{Max}} - \frac{\partial u^{(0)}}{\partial x}(x,t) & \text{if } \frac{\partial^2 u^{(0)}}{\partial t \partial x}(x,t) < 0. \end{cases} \quad (18)$$

Examples of the discontinuous function $H_0(x,t)$ for a pure monofrequency and a moderately distorted sinusoidal “simplex” wave forcing function are illustrated in Fig. 2.

Suppose the zeroth-order approximation of the local strain near x_0 , i.e.,

$$\frac{\partial u^{(0)}}{\partial x}(x_0+x,t) = \sum_{n=-\infty}^{+\infty} \varepsilon_n(x_0) e^{in(\omega_0/c_0)cq(n\omega_0)|x| - in\omega_0 t},$$

has a maximum ε_{Max} at t_{Max} and a minimum ε_{Min} at t_{Min} for $x = \Delta x$. Then

$$\begin{aligned} h_n = & \bar{\delta}_{n,0}[\varepsilon_{\text{Min}} + \varepsilon_{\text{Max}}](t_{\text{Min}} - t_{\text{Max}}) - \bar{\delta}_{n,0}\varepsilon_{\text{Min}} \frac{2\pi}{\omega_0} - 2\varepsilon_n \left(t_{\text{Min}} - t_{\text{Max}} - \frac{\pi}{\omega_0} \right) \\ & + (1 - \bar{\delta}_{n,0})[\varepsilon_{\text{Min}} + \varepsilon_{\text{Max}}] e^{-in(\omega_0/c_0)cq(n\omega_0)|\Delta x|} \cdot \frac{e^{in\omega_0 t_{\text{Min}}} - e^{in\omega_0 t_{\text{Max}}}}{in\omega_0} \\ & - 2 \sum_{m=-\infty}^{+\infty} (1 - \bar{\delta}_{n,m}) \varepsilon_m e^{-i(\omega_0/c_0)(n \cdot cq(n\omega_0) - m \cdot cq(m\omega_0))|\Delta x|} \cdot \frac{e^{i(n-m)\omega_0 t_{\text{Min}}} - e^{i(n-m)\omega_0 t_{\text{Max}}}}{i(n-m)\omega_0} \end{aligned} \quad (19)$$

with $\bar{\delta}_{ij} = 0$ if $i \neq j$ and $\bar{\delta}_{ij} = 1$ if $i = j$.

One easily recovers McCall and Guyer’s expressions when $\varepsilon_m = 0$ for $|m| \neq 1$, $\varepsilon_{\text{Max}} = -\varepsilon_{\text{Min}}$, $t_{\text{Min}} - t_{\text{Max}} = \pi/\omega_0$, and when no attenuation is taken into account. Equation (19), however, can be used in the iteration to calculate the distortion due to hysteresis at any distance as long as the wave satisfies the criteria of a simplex wave at that distance (i.e., being periodical with only one maximum and one minimum in one period of the strain).

When more than one maximum and minimum occur during a period (we refer to this as a “complex” wave), it means that the stress–strain relation experiences internal hysteresis loops within a larger loop. Figure 3 shows an example where two inner loops are formed on the descending stress–strain branch corresponding to two additional maxima and minima in the history of the forcing function. In order to find the hysteretic term in the modulus, one must keep track of all reversal points $\{t_m\}$ and of the end points of each inner loop $\{t'_m\}$ as shown in Fig. 3. The discontinuous function $H_0(x,t)$, which now also takes into account the additional local maxima and minima, becomes quite complicated to describe analytically. Perhaps Fourier analysis could still work in the most simple cases; however, once more and more extrema are formed the set of time reversal points and respective maxima and minima is difficult to keep track of

analytically. Approximating a function $H_0(x,t)$ such as the one illustrated in Fig. 3 requires the computation of a large number of Fourier coefficients. Even if one is capable of doing so, it remains a question as to whether it would be a worthwhile endeavor. Recall that we introduced the function

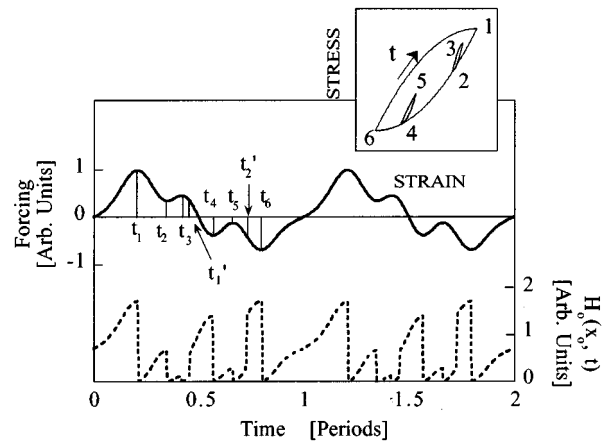


FIG. 3. Example of the function $H_0(x,t)$ for a highly distorted sinusoidal “complex” wave forcing function representative for an equation of state with internal stress–strain hysteresis loops (see inset). Here, $\{t_m\}$ and $\{t'_m\}$ are reversal and inner loop end points corresponding to discontinuities in the stress–strain relation.

$H_0(x,t)$ as an “analytic” approximation to the exact process given by P–M space. For complicated forcing functions the latter approximation may very well introduce a far larger error than a Fourier analysis representation. In this case we gain nothing by solving the problem in the Fourier domain because the function we started from does not describe the physics well. One alternative (and frankly it seems to be the only possibility) is to leave the analytic treatment and switch to a numerical approach that solves the differential equation in the time domain while linking to a numerical (tabulated) representation of the appropriate P–M space. This work is currently in progress.

II. EXAMPLES WITHIN THE LIMITATION OF SIMPLEX WAVES

In this section we illustrate some effects of hysteresis on the time waveform and frequency spectrum for conditions in which the above analytic treatment (within its limitations of simplex waves) can be applied. We begin this section with some examples of classical nonlinear theory using a Taylor series expansion of the stress–strain relation. Subsequently we illustrate the effects of introducing hysteresis. For clarity we will refer henceforth to the first-order (one parameter) Taylor series expansion as the β model [i.e., δ and ρ_B are both zero in Eqs. (6) and (7)], and to the extended second-order expansion as the β, δ model (i.e., ρ_B is zero). When hysteresis is taken into account in the model, we will use the term β, ρ_B model (δ will always be assumed zero in the β, ρ_B model examples). The nonlinearity parameters used in the model simulations will be indicated by the triplet $[\beta, \delta, \rho_B]$. In all of the examples the source function is a monofrequency continuous pressure wave of frequency f and displacement amplitude A . The propagation distance is 1 m except where noted otherwise. The linear sound velocity in the model is fixed at 2500 m/s and the linear attenuation corresponds to a quality factor (Q) of 50 except where noted. The number of distance iteration steps or finite difference back substitutions was set to 100, resulting in an acceptable calculation step size of 1 cm.

A. Classical nonlinear theory results

Figures 4–6 summarize results obtained from the classical nonlinear models. In Fig. 4(a) time waveforms are shown using the β model ($[\beta, \delta, \rho_B] = [-1000, 0, 0]$) for a single-frequency 10-kHz sinusoidal source at progressively larger amplitude levels. One observes an increased asymmetry with drive level and a correspondingly larger distribution of energy into harmonics as illustrated in Fig. 4(b). The harmonic energy in the spectral components tends to fall off rapidly (nearly exponentially) as a function of frequency. The nonlinear effect in this case is essentially frequency mixing between two spectral components: the double-frequency component is generated by a mixing of the fundamental with itself; the third harmonic arises by interaction of the second harmonic and the fundamental, etc. Figure 5, on the other hand, illustrates a threefold spectral component frequency mixing, resulting from the classical β, δ model with β equal to zero. The top figure shows the waveform calculations for a positive and negative value of the second nonlinearity pa-

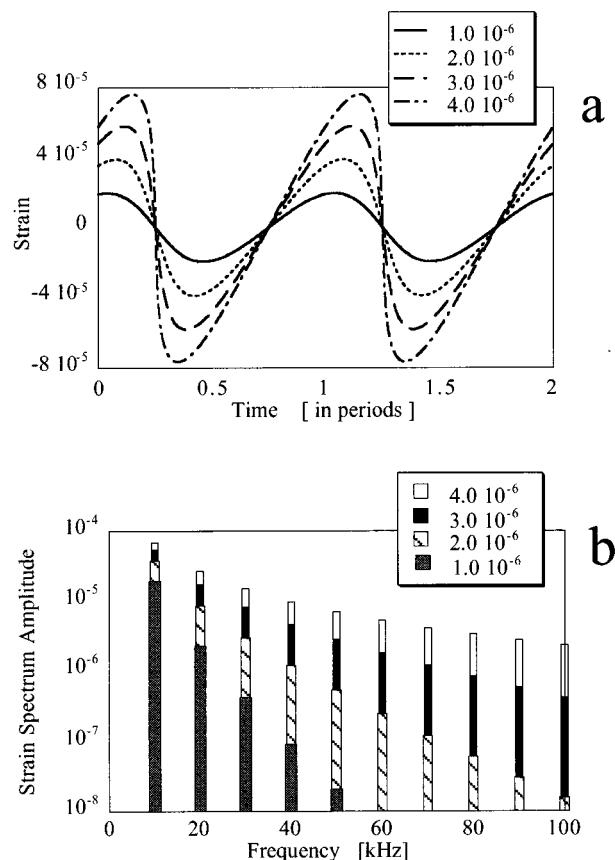


FIG. 4. (a) Strain waveforms from a sinusoidal monofrequency 10-kHz source signal after propagation of 1 m for different source displacement amplitudes (10^{-6} to 4.0×10^{-6} m, corresponding to strains of 2.5×10^{-5} to 10^{-4}). Model parameters: $[\beta, \delta, \rho_B] = [-1000, 0, 0]$. (b) Amplitude spectra for the waveforms shown in (a).

rameter ($[\beta, \delta, \rho_B] = [0, \pm 10^8, 0]$). In both cases, the distortion from a sinusoidal waveform is readily visible. The amplitude spectrum [Fig. 5(b)] is composed of odd harmonics only. This is the result of three-component mixing starting from a single-frequency source spectrum. That is, three fundamental frequencies can mix energy to form the third harmonic and corrections to the fundamental component. The third harmonic mixes with two fundamental components to form the fifth harmonic and so on. It is interesting that the frequency amplitude spectrum is identical for positive and negative δ values. The phase spectrum is different, however: the $(2m + 1)$ th spectral component for negative δ differs in phase from the $(2m + 1)$ th spectral component for positive δ by $m\pi$. This results in the mirror effect in the time history of the signal observed from Fig. 5(a). Figure 6 illustrates the result of combining the first and second nonlinearity parameter effects by fixing β and progressively increasing δ . The bold line in Fig. 6(a) shows the effect when $\delta = 0$. As in Fig. 5(a), positive δ values force the peak in the strain history to shift to earlier times, whereas negative values contribute to a shift to later times. Typically, absolute values for δ of one to two orders of magnitude larger than β^2 are required to notice differences in the distorted waveform. Characteristic spectra corresponding to a combination of first and second nonlinearity parameters are shown in Fig. 6(b). Due to the simu-

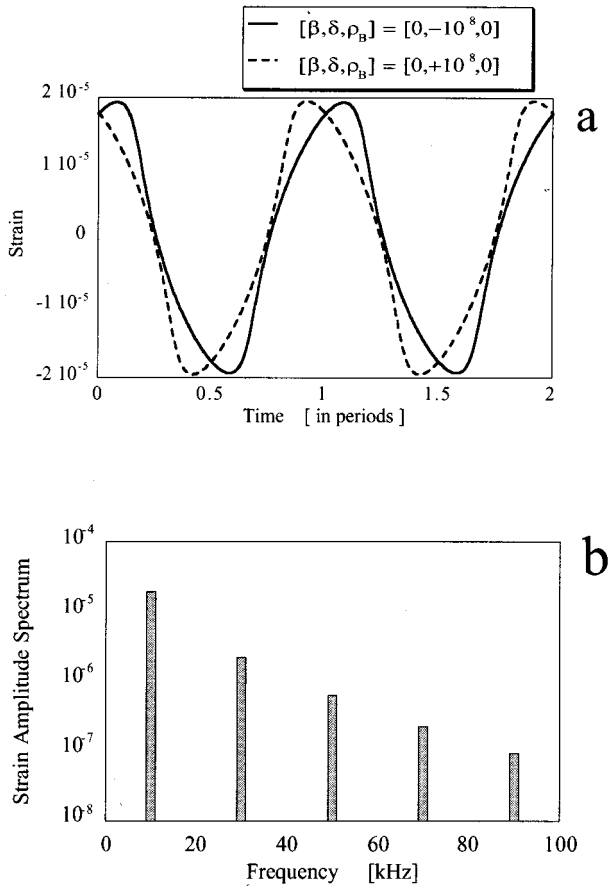


FIG. 5. (a) Strain waveforms from a sinusoidal monofrequency 10-kHz source signal with source displacement amplitude of 10^{-6} m after propagation of 1 m. Model parameters: solid line: $[\beta, \delta, \rho_B] = [-1000, -10^8, 0]$; dashed line: $[\beta, \delta, \rho_B] = [-1000, +10^8, 0]$. (b) Amplitude spectra for the waveforms shown in (a). The amplitude spectra are not influenced by the sign of δ .

taneous presence of two- and three-fold frequency interactions, one observes a richer spectrum with both even and odd harmonics present (as opposed to the case when $\beta=0$). Compared to the spectrum for $\delta=0$ [bars in Fig. 6(b)], we also note that more energy is pumped into the higher harmonics, increasing the higher frequency portion of the spectrum markedly. Because much energy can be transferred to odd harmonics by threefold frequency mixing δ contributions, a subsequent twofold mixing between an odd harmonic and the fundamental adds considerably to the energy content of its neighboring even components. In extreme cases this can lead to spectra which show a predilection for odd harmonics. We refer, for instance, to our previous papers for such observations and an attempt to model them using the classical nonlinear β, δ approach.^{15,18}

B. Quasi-analytic hysteretic approach

Figures 7 and 8 depict results from the quasi-analytic approach of the β, ρ_B model. We first illustrate the nonlinear effects introduced by the hysteretic coefficient without taking into account the nonlinearity parameter β . The waveform represented by the dashed line in Fig. 7(a) is a typical result of a purely hysteretic model. Because it is nearly triangular,

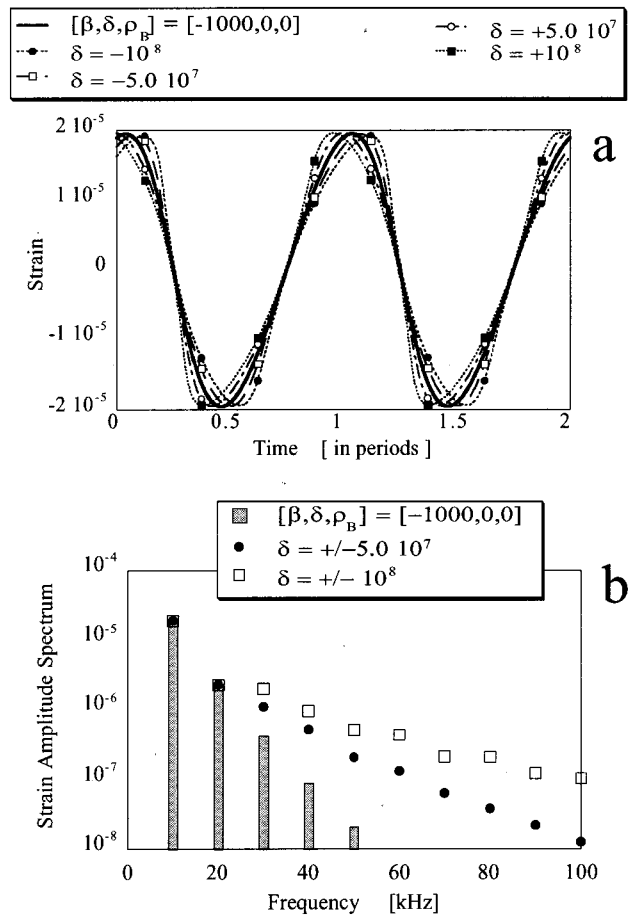


FIG. 6. (a) Strain waveforms from a sinusoidal monofrequency 10-kHz source signal with source displacement amplitude of 10^{-6} m after propagation of 1 m. Model parameters: bold line: $[\beta, \delta, \rho_B] = [-1000, 0, 0]$, others: $[\beta, \delta, \rho_B] = [-1000, -10^8, 0]$, $[-1000, -5 \cdot 10^7, 0]$, $[-1000, +5 \cdot 10^7, 0]$, $[-1000, +10^8, 0]$. (b) Amplitude spectra for the waveforms shown in (a). The amplitude spectra are not influenced by the sign of δ .

it consists of only odd harmonics [Fig. 7(b)]. The transformation of a smooth wave into a sawtooth form in hysteretic materials has also been noticed by Nazarov,²⁹ independently of our research. Mathematically one can explain this result as the twofold mixing between the fundamental source amplitude and a discontinuous function composed of only even harmonics which results from the analytic P-M space function $H_0(x, t)$ described in the above theory section. [The discontinuous function is composed of only even harmonics because it is periodic over half a source period as is illustrated in Fig. 2(a).] Compared to the linearly attenuated signal propagated over the same distance, one notes the strong generation of harmonics and a supplemental loss of energy due to hysteresis. We will return to the latter subject later. Figure 8 illustrates the combination of the first-order classical nonlinear theory with the hysteretic model for three different ρ_B values at fixed β ($[\beta, \delta, \rho_B] = [-1000, 0, 0]$, $[-1000, 0, 2000]$, $[-1000, 0, 4000]$). The waveforms become more and more symmetric (triangular) as ρ_B increases, diminishing the shock wave tendency effect imposed by the first nonlinearity parameter β . In addition, the strain amplitude becomes progressively reduced when compared to the classical result over the same propagation distance. Again, the combination

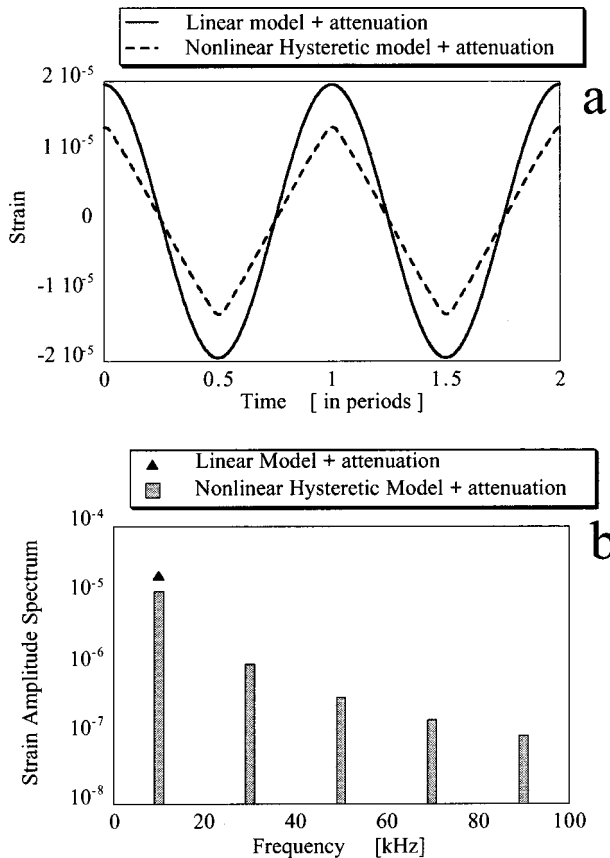


FIG. 7. (a) Strain waveform from a sinusoidal monofrequency 10-kHz source signal with source displacement amplitude of 10^{-6} m after propagation of 1 m (dashed line) and comparison with a purely linear signal with *ad hoc* attenuation. Model parameters for dashed waveform: $[\beta, \delta, \rho_B] = [0, 0, 4000]$. (b) Amplitude spectra for the linear and nonlinear waveforms shown in (a).

of twofold odd harmonic generation due to hysteresis and the classical twofold frequency mixing leads to rich spectra with a predilection for odd harmonics as illustrated in Fig. 8(b).

C. Local dynamic modulus

Using Eq. (6) one can calculate the local dynamic modulus at any distance from the source as a function of time or strain. Figure 9 shows the normalized local modulus after a propagation distance of 1 m as a function of time [Fig. 9(a)] and strain history at that same position [Fig. 9(b)] for examples of the three models considered. The normalization is performed with respect to the linear modulus, i.e., with respect to the modulus in the absence of any form of nonlinearity. Because the term $\delta(\partial u / \partial x)^2$ is either positive or negative depending on the sign of δ , its contribution causes an offset in the modulus–time and modulus–strain relation. The same is true for the hysteretic contribution which is always definite negative. Both classical models (β and β, δ approach) display a continuous variation of the modulus with time. The extended classical model shows more variation which is related to the richer frequency content at that distance. As a function of strain, the simple β model delineates a linear dependence with no discontinuities. The second-order β, δ model accounts for some curvature in the

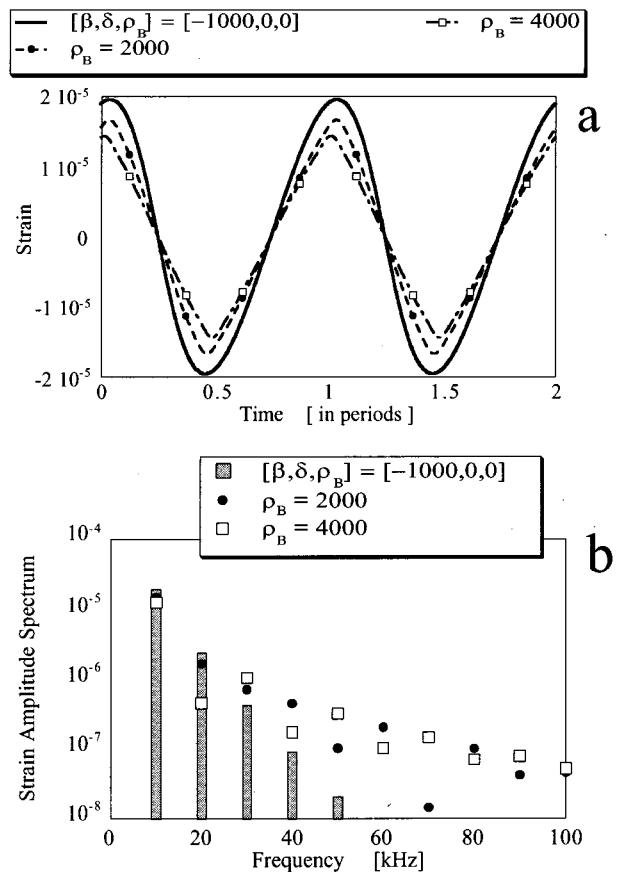


FIG. 8. (a) Strain waveforms from a sinusoidal monofrequency 10-kHz source signal with source displacement amplitude of 10^{-6} m after propagation of 1 m. Model parameters: bold line: $[\beta, \delta, \rho_B] = [-1000, 0, 0]$, others: $[\beta, \delta, \rho_B] = [-1000, 0, 2000]$, $[-1000, 0, 4000]$. (b) Amplitude spectra for the waveform shown in (a).

modulus–strain relation, but even in this case the modulus is continuous and single valued at every strain level. As explained in the theory section, hysteresis introduces a discontinuous term in the modulus which shows up in both its time and strain dependence. As a function of strain, the β, ρ_B model results in a multivalued modulus–strain relationship with a typical bow tie behavior. The modulus becomes discontinuous at peaks in the strain history, and differs for increasing or decreasing strain values. This type of discontinuous relationship is also a common observation in static experiments on rocks.^{4–6,22,23}

D. Hysteresis induced nonlinear attenuation

In Figs. 7 and 8 we noted that hysteresis contributes substantially to the nonlinear attenuation of a propagating wave. Given the same propagation distance, source frequency, and source amplitude, we plotted the maximum strain excursion (peak to peak) as a function of the hysteresis strength given by the parameter ρ_B in Fig. 10. The classical nonlinearity parameters β and δ are set equal to zero in order to emphasize on the contribution due to hysteresis only. The value at $\rho_B = 0$ corresponds to the linearly attenuated signal amplitude (i.e., $Q = 50$ and $[\beta, \delta, \rho_B] = [0, 0, 0]$), which is about 78% of the source amplitude measured peak to peak at 1 m

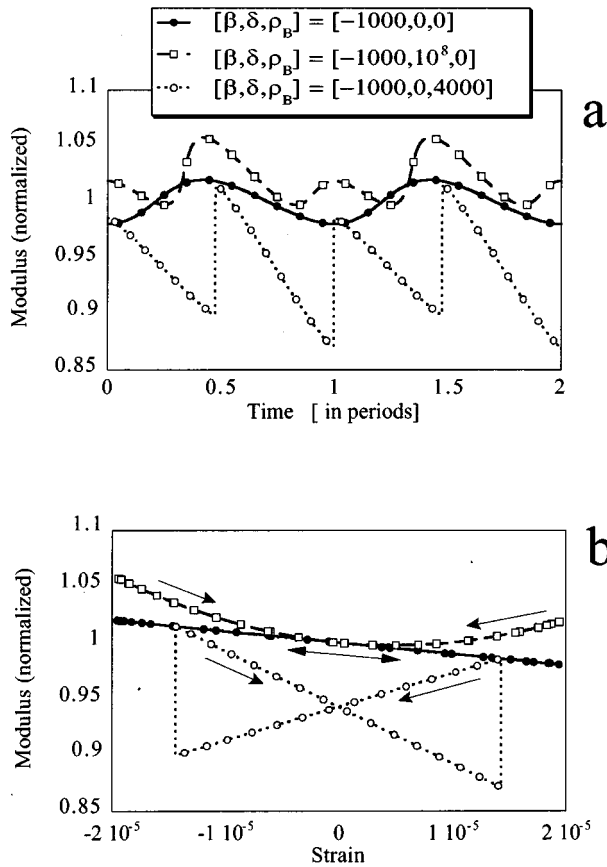


FIG. 9. Typical local dynamic (normalized) modulus–time (a) and modulus–strain (b) behavior for the three models. Normalization is with respect to the linear modulus (i.e., with respect to the modulus in the absence of any form of nonlinearity).

distance. For nonzero values of hysteretic strength, the amplitude monotonically decreases with increasing hysteresis. For instance, there is an additional 30% attenuation due to hysteresis for the model parameters $[\beta, \delta, \rho_B] = [0, 0, 5000]$, increasing the total attenuation to about 48% of the source signal.

Figure 11 illustrates the hysteretic damping characteristic in a somewhat different way. In a previous paper on the

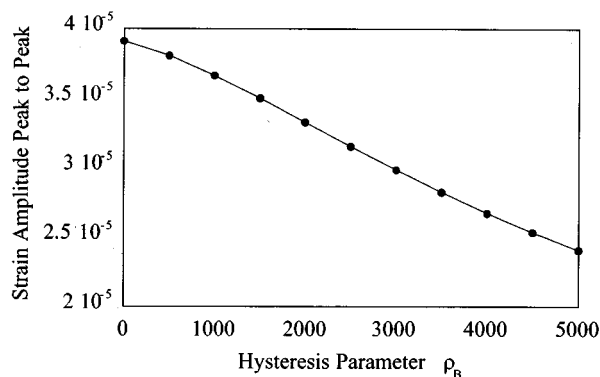


FIG. 10. Dependence of the peak-to-peak strain amplitude on the hysteresis strength for a sinusoidal monofrequency 10-kHz source signal with source displacement amplitude of 10^{-6} m after 1-m propagation distance (peak-to-peak strain at source $\approx 5 \times 10^{-5}$).

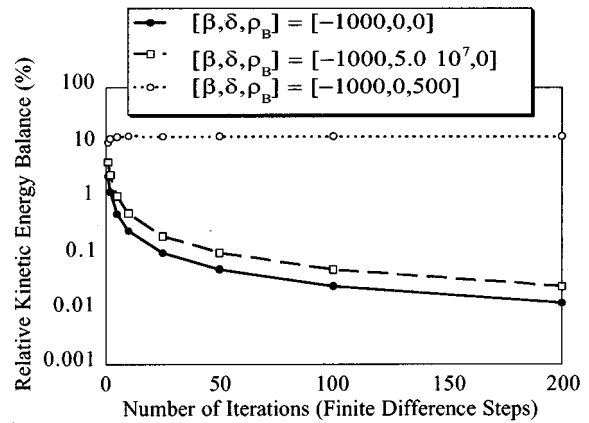


FIG. 11. Percentage of the relative kinetic energy balance [Eq. (20)] at 1-m propagation distance in the absence of attenuation ($Q=\infty$) as a function of number of iteration (finite difference steps) for the three models. Note that the relative kinetic energy balance is expressed in percentage.

discussion of the classical nonlinear theory¹⁷ we proved that the finite difference procedure provides a means of accounting for energy conservation in the absence of attenuation. To show this, we plotted the relative kinetic energy balance at distance L ,

$$\left| \frac{E_L - E_0}{E_0} \right| \cong \left| \frac{\sum_{n=-\infty}^{+\infty} |V_n(L)|^2 - \sum_{n=-\infty}^{+\infty} |V_n(0)|^2}{\sum_{n=-\infty}^{+\infty} |V_n(0)|^2} \right|, \quad (20)$$

as a function of the number of steps taken during the calculation. Here, E_0 and E_L are the kinetic energy at the source and at distance L , and $V_n = -in\omega_0 U_n$ are the spectral components of the velocity. The relative kinetic energy balance is a measure for energy loss integrated over the complete amplitude spectrum. Its value (zero or nonzero) determines whether energy is conserved or not. This should not be confused with the apparent losses in the fundamental due to harmonic generation. For the classical models (where $\rho_B \equiv 0$) and in the absence of linear attenuation, the theoretical value of the relative kinetic energy balance always corresponds to an energy excess ($E_L > E_0$), meaning that more energy is being transferred to harmonics than is being corrected for in the fundamental frequency. The relative error, however, decreases monotonically to acceptable values as the number of iterations is increased (solid circles and open squares in Fig. 11). The smaller the finite difference step, the more accurately energy conservation is satisfied in the model calculations. The results for the extended β, δ model decrease less rapidly than the simple β -approach due to the more pronounced higher harmonic generation. Classical nonlinear theory, in the absence of attenuation, thus preserves the total energy in the amplitude spectrum as a whole, even though losses can be noted in the amplitude of the fundamental due to nonlinear frequency mixing. Introducing hysteresis in the model reduces the kinetic energy at distance L significantly, resulting in an energy deficiency ($E_L < E_0$). In this case, the absolute value of the kinetic energy balance (open circles) asymptotically approaches a fixed nonzero value as the step-size decreases (13% for the model parameters chosen in this example). This is a clear indication that there is no energy

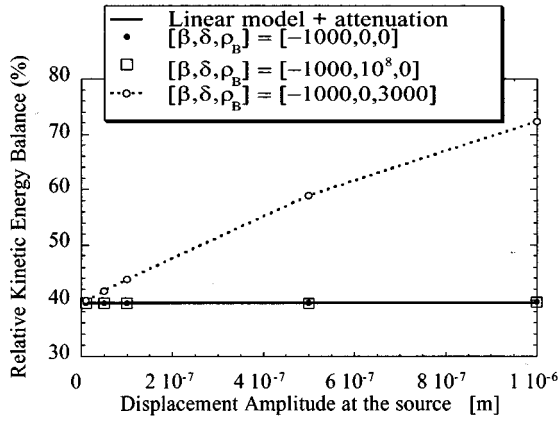


FIG. 12. Relative kinetic energy balance (in percentage) at 1-m propagation distance as a function of source displacement amplitude at 10 kHz for the linear and the three nonlinear models ($Q=50$).

conservation when hysteresis is present. Because classical nonlinearity does not cause energy reduction, we can state that hysteresis is responsible for all the “nonlinear energy loss” in a wave propagation experiment. Again, we emphasize that this loss should not be confused with the apparent nonlinear loss in the fundamental due to harmonic generation.

Analyzing the kinetic energy loss may thus be a simple manner by which to verify whether or not hysteresis is present in a material. We can illustrate this with one more figure. Given a quality factor $Q=50$, Fig. 12 shows the relative kinetic energy balance [Eq. (20)] for the classical models and the quasi-analytic hysteretic approach as a function of the displacement amplitude at the source. Both classical models do not significantly alter the kinetic energy balance as a function of amplitude. The only loss of energy in these cases is due to the linear attenuation. (The linear model and both classical models predict the same energy loss.) In the hysteresis model simulation, however, a clear linear dependence of kinetic energy loss with amplitude can be noted. The numerical calculations presented here are consistent with the analytic calculations by McCall and Guyer.²³ Thus, experimental verification of this observation somehow characterizes the role of hysteresis in the dynamic behavior of the sample. It simply requires the integration of the power spectrum of the velocity for different initial amplitudes at the source and at some propagation distance L . One can do this without any knowledge of the linear attenuation.

The order of magnitude of nonlinear attenuation and the manner in which it scales with ρ_B and strain amplitude can be understood from the following argument. A pressure cycle of amplitude ΔP carries a point in the material through a strain cycle of amplitude $\Delta \varepsilon$. From the expression of the inverse modulus [Eq. (4)], the associated strain hysteresis (e.g., measured at the midpoint of the pressure cycle) is

$$\begin{aligned} \partial \varepsilon &\approx \left(\frac{1}{M_{(p: -\Delta P \rightarrow \Delta P)}} - \frac{1}{M_{(p: \Delta P \rightarrow -\Delta P)}} \right) \Delta P \\ &= 2(\xi_0 \hat{\rho}_B \Delta P) \Delta P. \end{aligned} \quad (21)$$

Note that there is no influence of the classical nonlinearity

parameters. The associated irreversible energy loss is

$$\partial E \approx \partial \varepsilon \Delta P. \quad (22)$$

Since the energy “stored” in a pressure cycle, E_0 , is of order $\Delta \varepsilon \Delta P$, we have

$$\frac{1}{Q_{\text{Hyst}}} \approx \frac{\partial E}{E_0} \approx \frac{\partial \varepsilon}{\Delta \varepsilon} \approx 2\rho_B \Delta \varepsilon. \quad (23)$$

Here Q_{Hyst}^{-1} denotes the attenuation due to hysteresis effects. In arriving at the right-hand side we have used $M_2^2 \xi_0 \hat{\rho}_B = \rho_B$ and $\Delta P \approx M_2 \Delta \varepsilon$.

In Eq. (23) we see that the nonlinear attenuation is proportional to ρ_B and to $\Delta \varepsilon$. The proportionality of Q_{Hyst}^{-1} to ρ_B is demonstrated in Fig. 10; the proportionality of Q_{Hyst}^{-1} to $\Delta \varepsilon$ is demonstrated in Fig. 12.

Let us compare calculated strain levels in Fig. 10 with the levels deduced from the analysis of the amplitude reduction using Eq. (23). We focus on $\rho_B=5000$. The calculated strain amplitude (one-half peak-to-peak) at this value of hysteretic strength ($\Delta \varepsilon_{5000}$) is 1.2×10^{-5} . Also in Fig. 10 we see that the amplitude decreases (compared to the linear attenuated strain level $\Delta \varepsilon_0$) by an amount of order one, $(\Delta \varepsilon_0 - \Delta \varepsilon_{5000})/\Delta \varepsilon_0 \approx 0.4$, in traveling 1.0 m or 4 wavelengths. Using Eq. (23) we estimate the contribution to the nonlinear attenuation over that distance

$$\frac{1}{Q_{\text{Hyst}}} = \frac{\partial \varepsilon}{\Delta \varepsilon_0} \approx \frac{\Delta \varepsilon_0 - \Delta \varepsilon_{5000}}{\Delta \varepsilon_0} \approx 4 \cdot (2\rho_B \Delta \varepsilon_{\text{estim}}) \approx 0.4,$$

or $\Delta \varepsilon_{\text{estim}} \approx 1.0 \times 10^{-5}$, a strain in good agreement with the calculated value of 1.2×10^{-5} . Thus we find that Eq. (23) is qualitatively and quantitatively (order of magnitude) correct.

The results confirmed in this discussion suggest that the nonlinear attenuation can be regarded as a direct probe of ρ_B .

An important implication of energy loss due to hysteresis is that materials exhibiting hysteretic behavior such as certain rock and shape memory alloys could be used in building construction as supplementary damping layers for seismic activity.^{30,31} In the same context, it is also widely known that soils counteract soft surface layer resonance due to hysteresis induced energy losses.³² This becomes more and more important in site response studies for weak and strong motion in regions with conceivable damaging earthquake activity.

E. Dependence relations as guidance for inversion methods

Models can be very informative when used in a forward direction. However, a more interesting goal is to achieve a means of inverting the outcome of an experiment (or set of experiments) and to quantify the nonlinearity for characterization of the material. In the following we indicate some criteria that may help in the inversion process within the validity of simplex waves.

Assume three “virtual” materials, each of which satisfies the simulation by one of the three models considered in this paper: the simple β model, the extended classical β, δ approach, and the new β, ρ_B model. For simplicity we sup-

pose that the linear sound speed, linear attenuation, and the first nonlinearity parameter are the same for all three materials: $c_0=2500$ m/s, $Q=50$, and $\beta=-1000$.

First of all, we have shown in the above discussion of Figs. 10 and 12 that analyzing the kinetic energy loss may be a simple manner by which to verify whether or not hysteresis is present in a material.

In addition, an analysis of the time waveform and its frequency spectrum at a fixed propagation distance can provide a qualitative measure of the importance of the second nonlinearity parameter and of the hysteresis strength. Figures 4, 6, and 8 illustrate this for $[\beta, \delta, \rho_B]=[-1000, 0, 0]$, $[-1000, 10^8, 0]$, and $[-1000, 0, 4000]$, respectively. The presence of higher harmonics is an indication that some form of additional higher nonlinearity is necessary to describe the material's dynamic behavior. Furthermore, if the strain history takes on a typical triangular wave shape there is strong evidence that hysteresis is present.

Another way of obtaining information about the dominant nonlinear process (classical or hysteretic) is by looking at the individual spectral components and their dependence on distance, source frequency, and source amplitude. Recalling theoretical calculations by McCall,¹⁶ Van Den Abeele,¹⁷ and McCall and Guyer²³ for the propagation of a continuous monofrequency source signal in a nonlinear medium, we can summarize these elementary relationships for the second and third harmonic as follows:

(i) simple classical β models;

$$U_2 \propto \beta x f^2 U^2, \quad U_3 \propto \beta^2 x^2 f^4 U^3,$$

(ii) extended classical β, δ model:

$$U_2 \propto \beta x f^2 U^2,$$

$$U_3 \propto \beta^2 x^2 f^4 U^3 \quad \text{if } \frac{\beta^2 x f}{c_0} \gg \delta \quad \text{or}$$

$$U_3 \propto \delta x f^3 U^3 \quad \text{if } \frac{\beta^2 x f}{c_0} \ll \delta;$$

(iii) hysteresis β, ρ_B model:

$$U_2 \propto \beta x f^2 U^2,$$

$$U_3 \propto \beta^2 x^2 f^4 U^3 \quad \text{if } \frac{\beta^2 x f^2 U}{c_0^2} \gg \rho_B \quad \text{or}$$

$$U_3 \propto \rho_B x f^2 U^2 \quad \text{if } \frac{\beta^2 x f^2 U}{c_0^2} \ll \rho_B$$

(x is the distance to the source, f is the source frequency, U is the source displacement amplitude, and U_2, U_3 are the displacement amplitudes for the second and third harmonics at distance x).

These relationships are deduced in the absence of attenuation and apply for small propagation distances only. They also appear as the asymptotic behavior of our numerical calculation scheme using Eq. (16). In Figs. 13–15 we visualize these dependence relations for the second and third harmonic using the numerical simulations of the three model materials (under the conditions $\beta^2 x f \ll c_0 |\delta|$ and $\beta^2 x f^2 U \ll c_0^2 \rho_B$). (Note, however, that we plotted strain

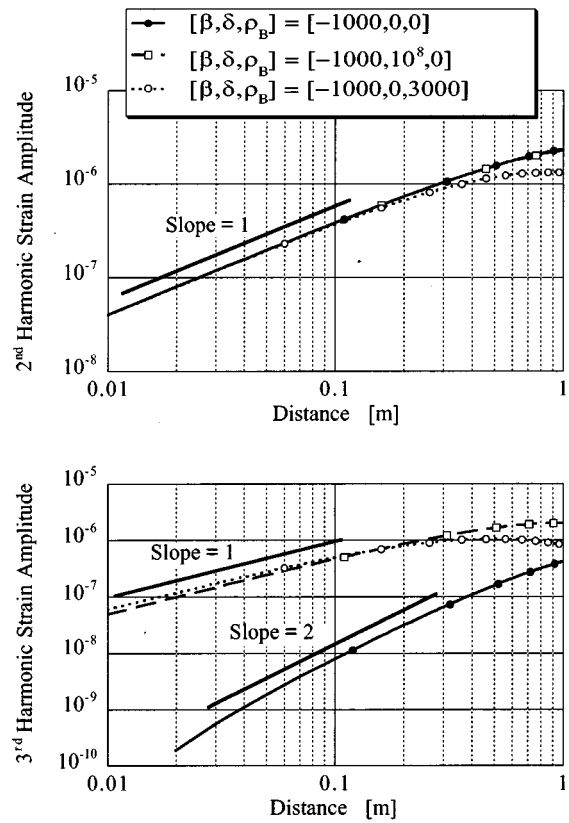


FIG. 13. Distance dependence of the second and third harmonic strain amplitudes for a sinusoidal monofrequency 10-kHz source signal with fixed source displacement amplitude of 10^{-6} m. Theoretical results for the three model materials.

amplitudes instead of displacement, which means that the power law dependence for frequency increases by 1 because $\epsilon_n \propto n f U_n$.) The behavior of the second harmonic as a function of distance, frequency, and amplitude does not provide comprehensible differentiation in the form of higher nonlinearity. Even in the presence of higher-order nonlinearity or hysteresis the classical dependence relations remain valid: the second harmonic is linearly dependent on the propagation distance, quadratic in source amplitude and source frequency, and the proportionality coefficient is a measure of the first nonlinearity parameter β . There is only a small difference when hysteresis is involved due to nonlinear attenuation. Study of the third harmonic, however, indicates significantly different behavior in the three model materials. A square law dependence for the distance (Fig. 13) of the third harmonic indicates that first-order nonlinearity dominates the dynamic behavior at this source frequency and amplitude. The observation of a linear dependence on distance indicates that either higher-order nonlinearity or hysteresis must be taken into account. Figure 14 tells us that the frequency dependence relation for the strain amplitude of third harmonic differs in all three models. Note, however, that this is only the case if the source displacement is kept constant at all frequencies. When strain amplitude is kept constant at the source, ϵ_3 is square law dependent on frequency in the β model and linearly proportional to frequency in the extended classical and hysteretic model. Figure 15 illustrates the

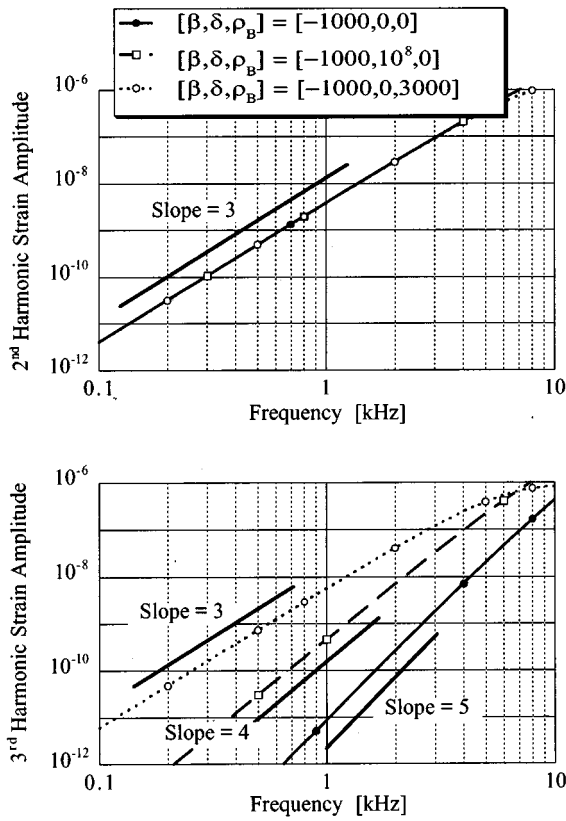


FIG. 14. Source frequency dependence of the second and third harmonic strain amplitudes for a sinusoidal monofrequency source signal with fixed source displacement amplitude of 10^{-6} m at 1-m propagation distance. Theoretical results for the three model materials.

source amplitude dependence (in displacement) for fixed frequency and propagation distance. The third harmonic strain amplitude satisfies a dependence on the source amplitude to the third power except when hysteresis is dominant in which case a square law relation applies.

In summary we can state that an analysis of the second harmonic is always restricted to information about the first-order nonlinear coefficient only. An evaluation of the third harmonic provides more insight into the dominant nonlinear characteristics. Given its dependence relations, third harmonic measurements can provide the clue as to whether the simple classical theory is sufficient, or if higher nonlinear constants or hysteresis must be considered.

We have only supplied some extreme characteristics. Real materials will usually have a nonlinear behavior that fall in between the theoretical bounds illustrated in this paper. Most certainly noninteger power law dependencies will be observed for real data, indicating that a combination of higher-order nonlinearity and hysteresis is present in the material. This is unquestionably the case for most rock for instance. That is why a large number of “basic” experimental data in the three-dimensional space of distance, frequency, and amplitude is necessary to perform a unique inversion within the limitations of this theory. In this context we also want to point out some experimental difficulties that are involved in obtaining such an extensive data set. Site response generally complicates corrections on distance measurements;

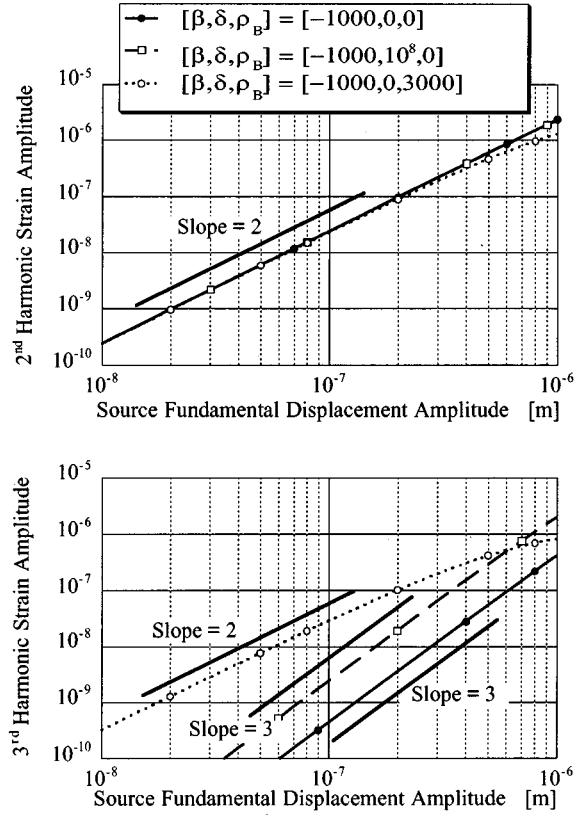


FIG. 15. Source amplitude dependence of the second and third harmonic strain amplitudes for a sinusoidal monofrequency 10-kHz source signal after 1-m propagation distance. Theoretical results for the three model materials.

the transfer function of the source transducer and receivers requires comprehensive deconvolution while stepping in frequency; and the generation of harmonics at the source with increasing drive level is a critical problem for the source amplitude dependence measurements.

Another important remark is that the theoretical model presented here is only a first-order approximation of the complex modeling that is involved based on the integral P–M space. The inversion for the triplet β , δ , and ρ_B only makes sense in the framework of this quasi-analytic treatment. These parameters are local and may depend strongly on the average pressure condition under which the experiment has been performed. Ultimately, we would like to arrive at a general description of the forward and backward models in terms of the global P–M space density $\rho(P_c, P_0)$. The local parameters β , δ , and ρ_B can then be readily obtained from this global density distribution.

III. CONCLUSION

A first-order approximation of the complex manifestation of hysteresis has been presented for the description of dynamic wave propagation in hysteretic materials by using an analytic expression for the modulus derived from P–M space modeling. The model is limited in validity to simplex waves, i.e., periodic waves with only one maximum and one minimum in one period of the strain. Within this limitation, the model illustrates that hysteretic effects can be identified

through a variety of experimental observations: triangular shaped waveform, predilection for odd harmonics, kinetic energy loss as a result of nonlinear attenuation, and particular source frequency and amplitude dependence relations for the third harmonic. Because hysteresis adds considerably to the attenuation of propagating waves, hysteretic materials can be used in basement constructions for large structures as additional effective damping layers counteracting seismic waves of large amplitude.

Even though this analytic description may only be a crude approximation of the complexity contained in the P–M space model of hysteresis, its simple implementation can be helpful in evaluating the applicability of classical nonlinear theory and in determining the strength of hysteresis in the material. The model will eventually be applied for inversion of experimental data sets to qualify and quantify the nonlinearity of the material in view of a new NDT characterization method.

ACKNOWLEDGMENTS

The authors thank J. A. Ten Cate, T. J. Shankland, A. Kadish, P. Rasolofosaon, and B. Zinszner for helpful discussions and valuable comments. This research is supported by NATO Scientific and Environmental Affairs (Advanced Fellowship for Koen Van Den Abeele), the Office of Basic Energy Science, Engineering and Geoscience under Contract No. W7405-ENG-36 with Los Alamos National Laboratory, by internal funds from Institutional Support, and the Institute of Geophysics and Planetary Physics.

- ¹D. J. Holcomb, "Memory, relaxation and microfracturing in dilatant rock," *J. Geophys. Res.* **86**, 6235–6248 (1981).
- ²C. H. Scholz and S. H. Hickman, "Hysteresis in the closure of nominally flat joints," *J. Geophys. Res.* **88**, 6501–6504 (1983).
- ³V. E. Nazarov, L. A. Ostrovsky, I. A. Soustova, and A. M. Sutin, "Nonlinear acoustics of micro-inhomogeneous media," *Phys. Earth Planet. Interiors* **50**, 65–73 (1988).
- ⁴G. N. Boitnott, "Fundamental observations concerning hysteresis in the deformation of intact and jointed rock with applications to nonlinear attenuation in the near source region," in *Proceedings of the Numerical Modeling of Underground Nuclear Test Monitoring Symposium*, Durango, CO, 1993, edited by S. R. Taylor and J. R. Kamm, Los Alamos National Laboratory Report (LA-UR-93-3839), 1993.
- ⁵G. A. Gist, "Fluid effects on velocity and attenuation in sandstones," *J. Acoust. Soc. Am.* **96**, 1158–1173 (1994).
- ⁶L. B. Hilbert, Jr., T. K. Hwang, N. G. W. Cook, K. T. Nihei, and L. R. Myer, "Effects of strain amplitude on the static and dynamic nonlinear deformation of Berea sandstone," in *Rock Mechanics Models and Measurements: Challenges From Industry*, edited by P. P. Nelson and S. E. Laubach (Balkema, Rotterdam, 1994), pp. 497–504.
- ⁷R. A. Guyer, K. R. McCall, and G. N. Boitnott, "Hysteresis, discrete memory and nonlinear wave propagation in rock: a new paradigm," *Phys. Rev. Lett.* **74**, 3491–3494 (1994).
- ⁸R. A. Guyer, K. R. McCall, P. A. Johnson, P. N. J. Rasolofosaon, and B. Zinszner, "Equation of state hysteresis and resonant bar measurements on rock," in *1995 International Symposium on Rock Mechanics*, edited by J. J. K. Daemon and R. A. Schultz (Balkema, Rotterdam, 1995), pp. 177–181.
- ⁹J. Ortin, "Preisach modeling of hysteresis for a pseudoelastic Cu–Zn–Al single crystal," *J. Acoust. Soc. Am.* **71**, 1454–1461 (1992).
- ¹⁰H. H. Law, P. L. Rossiter, G. P. Simon, and J. Unsworth, "A model for the structural hysteresis in poling and thermal depoling of PZT ceramics," *J. Mater. Sci.* **30**, 4901–4905 (1995).
- ¹¹S. A. Mansour, G. L. Liedl, and R. W. Vest, "Microstructural developments and dielectric properties of rapid thermally processed PZT thin-films derived by metalloorganic decomposition," *J. Am. Ceram. Soc.* **78**, 1617–1623 (1995).
- ¹²F. D. Murnaghan, *Deformation of an Elastic Solid* (Wiley, New York, 1951).
- ¹³L. D. Landau and E. M. Lifshitz, *Theory of Elasticity* (Pergamon, Oxford, 1959).
- ¹⁴L. K. Zarembo and V. A. Krasil'nikov, "Nonlinear phenomena in the propagation of elastic waves in solids," *Sov. Phys. Usp.* **13**, 778–797 (1971) (in English).
- ¹⁵G. D. Meegan, P. A. Johnson, R. A. Guyer, and K. R. McCall, "Observations of nonlinear elastic wave behavior in sandstone," *J. Acoust. Soc. Am.* **94**, 3387–3391 (1993).
- ¹⁶K. R. McCall "Theoretical study of nonlinear elastic wave propagation," *J. Geophys. Res.* **99**, 2591–2600 (1994).
- ¹⁷K. E. Van Den Abeele, "Elastic pulsed wave propagation in media with second or higher order nonlinearity. Part I. Theoretical framework," *J. Acoust. Soc. Am.* **99**, 3334–3345 (1996).
- ¹⁸K. E. Van Den Abeele and P. A. Johnson, "Elastic pulsed wave propagation in media with second or higher order nonlinearity. Part II. Simulation of experimental measurements on Berea sandstone," *J. Acoust. Soc. Am.* **99**, 3346–3352 (1996).
- ¹⁹J. A. Ten Cate, K. Van Den Abeele, T. J. Shankland, and P. A. Johnson, "Laboratory study of linear and nonlinear elastic pulse propagation in sandstone," *J. Acoust. Soc. Am.* **100**, 1383–1391 (1996).
- ²⁰P. A. Johnson, B. Zinszner, and P. N. J. Rasolofosaon, "Resonance and nonlinear elastic phenomena in rock," *J. Geophys. Res.* **101**(B5), 11 553–11 564 (1996).
- ²¹P. A. Johnson and P. N. J. Rasolofosaon, "Manifestation of nonlinear elasticity in rock: convincing evidence over large frequency and strain intervals from laboratory studies," *Nonlinear Proc. Geophys.* **3**, 77–88 (1996).
- ²²K. R. McCall and R. A. Guyer, "Hysteresis, discrete memory and nonlinear elastic wave propagation in rock: a new theoretical paradigm," *Nonlinear Proc. Geophys.* **3**, 89–101 (1996).
- ²³K. R. McCall and R. A. Guyer, "Equation of State and wave propagation in hysteretic nonlinear elastic materials," *J. Geophys. Res.* **99**, 23 887–23 897 (1994).
- ²⁴J. B. Walsh, "The effect of cracks on the compressibility of rocks," *J. Geophys. Res.* **70**, 381–389 (1965); "The effect of cracks on the uniaxial elastic compression of rocks," *J. Geophys. Res.* **70**, 399–411 (1965).
- ²⁵F. Preisach, "Über die Magnetische Nachwirkung," *Z. Phys.* **94**, 277–302 (1935).
- ²⁶J. D. Mayergoyz, "Hysteresis models from the mathematical and control theory points of view," *J. Appl. Phys.* **57**, 3803–3805 (1985).
- ²⁷F. M. Pestorius and D. T. Blackstock, "Propagation of finite amplitude noise," in *Finite amplitude wave effects in fluids, Proceedings of the 1973 Symposium*, edited by L. Bjorno (Copenhagen, DK, 1973) (IPC Science and Technology Press Ltd., Westbury House, Guildford, England, 1973), pp. 24–29.
- ²⁸M. E. Haran and B. D. Cook, "Distortion of finite amplitude ultrasound in lossy media," *J. Acoust. Soc. Am.* **73**, 774–779 (1983).
- ²⁹V. Nazarov, "Propagation of a unipolar impulse in a medium with hysteretic nonlinearity," preprint IAP n.383, N. Novgorod, 1995, (in Russian), submitted to *Akust. Zh.*
- ³⁰J. M. Kelly, "Application of shape memory materials for reduction of structural response to earthquake ground motion," *Proceedings of the Workshop on Smart and High Performance materials and structures*, Tskuba, Japan (May 1993).
- ³¹P. W. Clark, I. D. Aiken, J. M. Kelly, M. Higashino, and R. Krumme, "Experimental and analytical studies of shape memory alloys dampers for structural control," in *Smart Structures and Materials 1995: Industrial and commercial applications of smart structures technologies*, 2–3 March 1995, San Diego, CA, edited by C. R. Crowe (Bellingham, WA, 1995).
- ³²I. A. Beresnev and K.-L. Wen, "Nonlinear soil response—A reality?," *Bull. Seis. Soc. Am.* **86**(6), 1964–1978 (1996).